JOURNAL OF THE MECHANICAL BEHAVIOR OF BIOMEDICAL MATERIALS ▮ (▮▮▮▮) ▮▮▮–▮▮▮

Available online at www.sciencedirect.com

ScienceDirect

www.elsevier.com/locate/jmbbm

Research Paper

Modeling the biomechanical and injury response of human liver parenchyma under tensile loading

*Costin D. Untaroiu**, *Yuan-Chiao Lu*, *Sundeep K. Siripurapu*, *Andrew R. Kemper*

Virginia Tech and Wake Forest University School of Biomedical Engineering and Sciences, Blacksburg, VA 24060, USA

ARTICLE INFO

Article history:
Received 1 April 2014
Received in revised form
2 July 2014
Accepted 4 July 2014

Keywords:
Human liver
Parenchyma
Failure
Tensile test
Material model
Cohesive zone Model
Finite element
Optimization

ABSTRACT

The rapid advancement in computational power has made human finite element (FE) models one of the most efficient tools for assessing the risk of abdominal injuries in a crash event. In this study, specimen-specific FE models were employed to quantify material and failure properties of human liver parenchyma using a FE optimization approach. Uniaxial tensile tests were performed on 34 parenchyma coupon specimens prepared from two fresh human livers. Each specimen was tested to failure at one of four loading rates ($0.01\,s^{-1}$, $0.1\,s^{-1}$, $1\,s^{-1}$, and $10\,s^{-1}$) to investigate the effects of rate dependency on the biomechanical and failure response of liver parenchyma. Each test was simulated by prescribing the end displacements of specimen-specific FE models based on the corresponding test data. The parameters of a first-order Ogden material model were identified for each specimen by a FE optimization approach while simulating the pre-tear loading region. The mean material model parameters were then determined for each loading rate from the characteristic averages of the stress–strain curves, and a stochastic optimization approach was utilized to determine the standard deviations of the material model parameters. A hyperelastic material model using a tabulated formulation for rate effects showed good predictions in terms of tensile material properties of human liver parenchyma. Furthermore, the tissue tearing was numerically simulated using a cohesive zone modeling (CZM) approach. A layer of cohesive elements was added at the failure location, and the CZM parameters were identified by fitting the post-tear force–time history recorded in each test. The results show that the proposed approach is able to capture both the biomechanical and failure response, and accurately model the overall force–deflection response of liver parenchyma over a large range of tensile loadings rates.

*Corresponding author. Tel.: +1 540 231 8997; +fax: +1 540 231 2953.
E-mail address: costin@vt.edu (C.D. Untaroiu).

http://dx.doi.org/10.1016/j.jmbbm.2014.07.006
1751-6161/

1. Introduction

Liver injuries frequently caused by both frontal and side impact motor vehicle collisions are associated with high morbidity and mortality rates (Nahum and Melvin, 2002). Capsule lacerations and parenchyma damage are common liver injuries and could be severe (Harbrecht et al., 2001). Injury mechanisms of blunt liver trauma, such as deceleration injury and crush injury, have been proposed in the literature (Jin et al., 2013; Ahmed and Beckingham, 2007). However, these injury mechanisms are primarily dependent on the injury location observed in medical images, and the assumed direction and location of applied force during the crash. Recent experimental studies (Howes et al., 2012) have investigated the relative kinematics of the thoraco–abdominal organs during dynamic blunt loading using high-speed biplane x-ray technology. While the results were promising, the limited field of view and simplified loading conditions make a complete understanding of liver injuries challenging. Human finite element (FE) models have the capability to simulate each time step during an impact event and calculate the stress/strain field within human organs that could be correlated with injuries. However, the FE predictions are highly dependent on the model geometries, the connections of its parts, and especially the assigned material properties. Therefore, to numerically investigate liver injuries, biofidelic material properties are needed over a large range of loading rates.

Several studies have investigated the failure properties of liver parenchyma in uniaxial tension using animal specimens: bovine (Santago et al., 2009a, 2009b; Lu et al., 2014) porcine (Hollenstein et al., 2006; Chui et al., 2007; Brunon et al., 2010) and rabbit (Yamada, 1970). Recently, an extensive study presented the results of a total of 51 tensile tests performed on human liver parenchyma at four loading rates (Kemper et al., 2010). The stress–strain curves until failure were obtained using load cells, pre-test pictures, high-speed video, and optical markers placed on the specimens. Although these previous studies provide considerable insight into the factors that affect the tensile response of liver parenchyma, the strain time histories were usually obtained from the local marker displacements. Additionally, FE material models, with verification in terms of global properties of entire specimens, were not developed based on the experimental test data.

The primary goal of this study was to accurately model both the biomechanical and failure responses of human liver parenchyma under tensile loading. To identify the parameters of a non-linear material model assigned to liver parenchyma, specimen-specific FE models and a simulation-based optimization approach were employed as in other recent studies (Hu et al., 2009, 2011; Untaroiu, 2013; Untaroiu and Lu, 2013; Lu et al., 2013). Then, the average stress–strain curves and failure properties developed based on specimen-specific FE models were compared to local marker data. To model the tear of the liver parenchyma, the Cohesive Zone Modeling (CZM) approach, implemented recently in most FE software packages, was utilized to model the pre- and post-failure behavior of parenchyma coupon specimens. The data reported in the current study could be easily implemented in current human liver models (Behr et al., 2003; Vavalle et al., 2013). Then, a better understanding of liver injury mechanisms could be obtained using biofidelic human models in numerical impact simulations.

2. Methods

2.1. Experimental testing

Uniaxial tensile tests were performed on the parenchyma of two fresh human livers. Thirty-four "dog-bone shape" specimens were prepared using the custom blade assembly, slicing jig, and stamp described in previous studies (Kemper et al., 2010; Lu et al., 2013, 2014; Untaroiu and Lu, 2013). The length, width, and thickness of the gage length were approximately 55.5 mm, 10 mm, and 5 mm respectively. The liver parenchyma specimens did not contain any visible defects, vasculature, or the capsule. The longitudinal direction (or "loading direction") of the specimens was parallel to the surface of the liver. Prior to testing, specimens were immersed in a bath of Dulbecco's Modified Eagle Medium (DMEM) to maintain specimen hydration. It should be mentioned that one previous study (Santago et al., 2009b) found no statistically significant changes in failure tensile stress or strain between specimens tested at normal room temperature (24 °C) and body temperature (37 °C). Therefore, the human liver parenchyma was tested at a normal room temperature (24 °C), and within 48 h of death to minimize the effects of tissue degradation (Lu and Untaroiu, 2013).

The testing system consisted of two motor driven linear stages (Parker Daedal MX80S, Irwin, PA) mounted to a vertically oriented aluminum plate (Fig. 1). The specimen

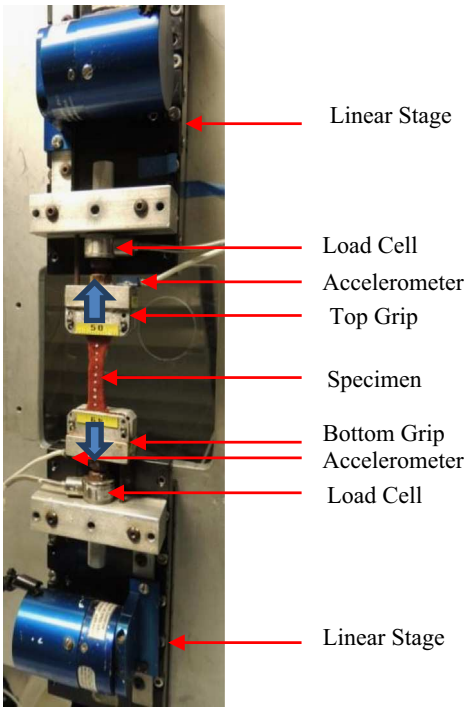

Fig. 1 – Experimental setup.

Please cite this article as: Untaroiu, C.D., et al., Modeling the biomechanical and injury response of human liver parenchyma under tensile loading. Journal of the Mechanical Behavior of Biomedical Materials (2014), http://dx.doi.org/10.1016/j.jmbbm.2014.07.006

Table 1 – Data Acquisition and high-speed video sampling rates by loading rate

Rate	Number of specimens	Desired strain rate (s^{-1})	Data acquisition (kHz)	High-speed video (Hz)
1	7	0.01	0.2	20
2	9	0.1	2	70
3	9	1.0	20	500
4	9	10	40	1000

mounting procedure was used to ensure that all specimens had a minimal but consistent preload (i.e. 1 g of tension) (Kemper et al., 2010; Lu et al., 2013, 2014). The specimen was aligned so that the longitudinal axis of the specimen coincided with the centerline of the load train. Prior to each test, the 3-dimensional geometry of each specimen mounted between clamps was obtained using a FARO Laser Scanner (Laser Line Probe V3, FARO Technologies, Inc., Lake Mary, Florida) with an accuracy of $\pm 35\,\mu m$. In addition, a collinear and equidistant pattern of paint (optical) markers was applied to each specimen (Fig. 1) prior to testing with 4 mm between each marker. A high speed video camera (Phantom V9, Vision Research, Wayne, NJ) with a resolution of 7.7 pixels/mm recorded the specimen-response during testing (Table 1). The testing system loaded the specimen by simultaneously moving the top and bottom grips away from one another at a constant velocity. All the specimens were divided into four groups, and tested until complete failure at one of the following four strain rates: 0.01 s^{-1}, 0.1 s^{-1}, 1 s^{-1}, or 10 s^{-1} (Table 1).

The displacement between grips was measured using potentiometers attached to the linear stages and was then fitted with a 1st degree polynomial to reduce the measurement noise. The time history of force measured at the load cell was inertially compensated and then fitted by a 5th degree polynomial up to the time of failure (average $R^2=0.902$). The tissue failure was defined as the point on the force–time curve where the force reached a maximum and then decreased more than 3% of the peak value. The corresponding time was defined as the "time of failure".

2.2. Constitutive characterization of the human parenchyma tissue

2.2.1. The marker model

The marker model utilizes the constant cross-sectional area and the displacement of the two markers adjacent to the failure site. The displacement between the closest optical markers adjacent to the tear was tracked in the video until failure using motion analysis software (TEMA Version 2.6, Linkoping, Sweden). To reduce the inherent noise, the displacement was curve fit with a 5th degree polynomial (average $R^2=0.999$). The local stretch ratio (λ) and Green–Lagrangian (GL) strain (ε) were calculated from the curve fit displacement data as follows:

$$\lambda = \frac{L_n}{L_0} \tag{1}$$

$$\varepsilon = \frac{1}{2}(\lambda^2 - 1) \tag{2}$$

where L_0 is the original distance between the optical markers, and L_n is the instantaneous distance between the optical markers. The 2nd Piola–Kirchhoff (PK) Stress (S) was then calculated based on the inertially compensated force data (F_e), stretch ratio (λ), and initial cross-sectional area (A_0) as follows:

$$S = \frac{F_e}{\lambda A_0} \tag{3}$$

The force vs. deformation (displacement between grips) and stress vs. strain data using the marker model were combined with similar previously published human liver parenchyma data obtained from three fresh human livers (Lu et al., 2013), resulting in a total of eighty-six specimens. The average force-deformation curves, average strain-stress curves, and corresponding variation corridors at each strain rate were calculated from this combined dataset. Average curves were computed using a normalizing technique, and the boundaries of the corridor data were defined along the average curves using ± 1 standard deviation (SD) as ellipsoidal axes (Untaroiu and Lu, 2013).

2.2.2. The specimen-specific FE model

Poly-surfaces of the specimens were constructed using Geomagic Studio 11 (Geomagic Inc., Morrisville, NC) based on the point clouds recorded prior to testing with the FARO Laser Scanner. These data were transformed into Non-Uniform Rational B-spline (NURBS) surfaces using Rhino vers.5.0 (Robert McNeel & Associates, Seattle, WA), which were then used in meshing. Specimen-specific FE models were developed for each specimen using a structural meshing approach in TrueGrid vers. 2.3.4. (XYZ Scientific Applications, Livermore, CA). In a previous study, a mesh with approximately 400 hexahedral elements showed a good convergence in these loading conditions (Untaroiu and Lu, 2013). Therefore, a similar mesh density was used in the current study. Finally, a uniform smoothing algorithm (Rainsberger, 2006) was used to automatically improve the mesh quality of the hexahedral elements (e.g. jacobian, aspect ratio, etc.).

Many previous studies showed that an isotropic hyper-elastic formulation reasonably approximates the nonlinear behavior of abdominal solid organ tissues (Gao et al., 2010; Umale et al., 2013; Snedeker et al., 2005). Therefore, a commonly used hyper-elastic formulation, the Ogden material model, implemented in the FE software (LS-Dyna vers. 6.0, LSTC, Livermore, CA) was assigned to specimen-specific FE models. This material model (LS-Dyna MAT_77 (Hallquist, 2006)) has an unconstrained form due to a hydrostatic work term to the strain energy function:

$$W(\lambda_1,\lambda_2,\lambda_3) = \sum_{i=1}^{N} \frac{\mu_i}{\alpha_i}(\lambda_1^{\alpha_i} + \lambda_2^{\alpha_i} + \lambda_3^{\alpha_i} - 3) + K(J - 1 - \ln J) \tag{4}$$

where K is the bulk modulus and J is the volume ratio. The liver parenchyma was assumed to be a nearly incompressible

Please cite this article as: Untaroiu, C.D., et al., Modeling the biomechanical and injury response of human liver parenchyma under tensile loading. Journal of the Mechanical Behavior of Biomedical Materials (2014), http://dx.doi.org/10.1016/j.jmbbm.2014.07.006

material, with a Poisson's ratio of 0.4996 in all models. Each tension test was simulated by prescribing the displacement-time histories, recorded during testing, to the specimen ends. In the implicit simulations ($0.01\,s^{-1}$ and $0.1\,s^{-1}$ strain rates), a fully integrated element integration scheme was used. A constant stress element formulation with a viscosity-based hourglass control ($Q_m=0.02$) was used in all explicit simulations ($1\,s^{-1}$ and $10\,s^{-1}$ strain rates). A simulation was considered successful if the peak hourglass energy was less than 3% of the peak internal energy.

The first-order Ogden material parameters, μ_1 and α_1, were identified using a metamodel-based optimization, called the sequential response surface method (SRSM), implemented in LS-Opt software. This iterative method uses a region of interest, which changes in size after each iteration, to determine an approximate optimum. The root-mean-square (RMS) of the difference between the experimental force data and corresponding simulated model data was defined as the objective function to be minimized. A D-optimal design was used to assign test points around the optimum point which is determined after each iteration. Subsequently, a quadratic response surface was fitted through the values of the objective function calculated from the corresponding FE simulations. The initial values of the Ogden parameters were obtained using an analytical model for each specimen (Untaroiu and Lu, 2013; Lu et al., 2013), and the optimization process was stopped after six iterations. The maximum GL strain along the tensile direction at the time of failure obtained from testing was defined as the GL failure strain. Then, the stretch ratio and 2nd PK stress at failure were derived using failure GL strain and the optimized Ogden material parameters.

The stress–strain relationships calculated from the optimized Ogden material parameters were used to compute average curves and variation corridors for each strain rate using the corridor approach mentioned previously (Untaroiu and Lu, 2013). The average Ogden material parameters for each strain rate were identified using the average curves of the specimen-specific FE model data by an optimization-based approach performed in Matlab vers. R2012b (MathWorks, Inc., Natick, MA). In addition, the corresponding SD of the model parameters for each strain rate were also identified using a stochastic optimization approach performed in Matlab (Lu et al., 2013). The average 2nd PK stress vs. GL strain curves were transformed to engineering stress vs. engineering strain and then used as inputs of a LS-Dyna material model, MAT_181 (*MAT_SIMPLIFIED_RUBBER/FOAM). This LS-Dyna material model uses a tabulated formulation of hyperelasticity with rate effects (Kolling et al., 2007). The accuracy of this material model was tested using a simple cube element (Fig. 2(a)) loaded at each of four strain rates used in this study, and three other intermediate strain rates.

Various computational methods have been proposed for modeling dynamic fracture of engineering materials (Cox et al., 2005). The cohesive zone theory is a popular method that has shown promising results in modeling the failure propagation through various engineering materials. This method considers fracture as a gradual process of separation by adding an interface in the region adjacent to the tip of the forming crack (Kanninen and Popelar, 1985; Park and Paulino, 2013). In this study, a cohesive zone model (CZM) interface, consisting of hexahedral elements with zero height, was inserted transversally at the location of the observed tear (Fig. 2(b)) in four specimens corresponding to high strain rate tests (Rate 3: L3-01_4, L3-02_4 Rate 4: L4-01_4, L4-02_4) to model the tissue tearing process. Similar to the constitutive (stress–strain) relationships used to model the tissue (bulk) material, CZM requires a traction separation law to be prescribed for the tear propagation path (Fig. 3(a)).

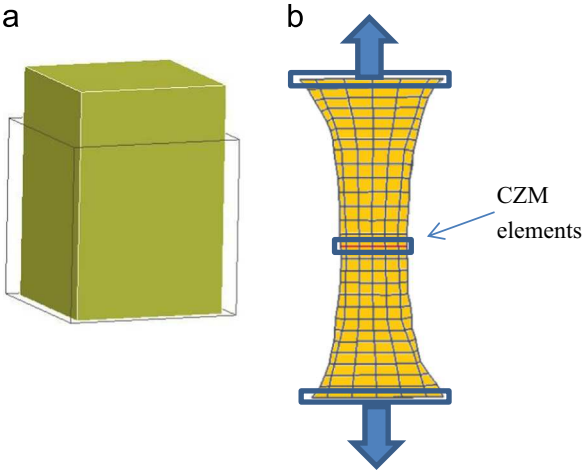

Fig. 2 – (a) Single cube element used to verify the FE material model in tension (b) The specimen model with a CZM defined at the tear location.

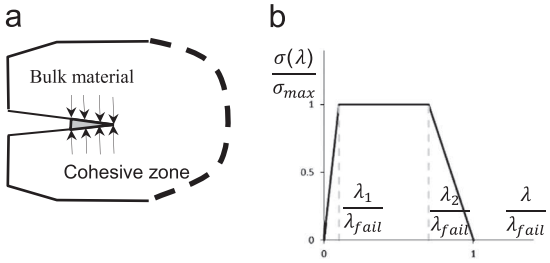

Fig. 3 – (a) Schematic of cohesive zone model. (b) Effective traction–separation relationship (Tvergaard and Hutchinson 1992).

Various traction–separation relationships have been proposed in the literature such as cubic polynomial (Tvergaard, 1990), trapezoidal (Tvergaard and Hutchinson, 1992, 1993), exponential (Ortiz and Pandolfi, 1999; Benzeggagh and Kenane, 1996), linear softening (Camacho and Ortiz, 1996), and bilinear softening (Guinea et al., 1994). A material model implemented in LS-Dyna (MAT_185, *MAT_COHESIVE_TH) with a normalized trapezoidal traction–separation relationship (Fig.3(b)) was used in the definition of the CZM part (Fig. 2(b)). In this material formulation, the peak traction (the force over area $-\sigma_{max}$) reached at a separation of λ_1 is kept constant (ductile behavior) until the separation reaches λ_2. Then, a linear reduction of the traction (elastic softening response) is simulated until a separation of λ_{fail} is reached, which corresponds to when the damage is complete.

Since CZM is defined to simulate the failure modes generated by both tensile (mode I) and shear stresses (modes

II and III), the effective separation λ is expressed in terms of the normal (δ_n) and tangential (δ_t) components of the displacement at the cohesive interface

$$\lambda = \sqrt{\left(\frac{\delta_n}{\delta_n^c}\right)^2 + \left(\frac{\delta_t}{\delta_t^c}\right)^2} \quad (5)$$

where δ_n^c and δ_t^c are critical values of the normal and tangential characteristic components.

An additional optimization was setup to match the experimental and numerical force time histories for both pre- and post-failure regimes. The CZM parameters (λ_1, λ_2, λ_{fail}, δ_n^c, σ_{n_max}) were considered as input variables. Since the specimen is loaded primarily in tension, the tearing occurs as failure mode I. Therefore, the CZM parameters corresponding to shear loading have a negligible influence on the tear propagations, so their unknown values (δ_t^c, σ_{t_max}) were assigned to be equal to the corresponding values in tension. Since the addition of CZM influences only the timing of tear occurrence and post-failure behavior, not the pre-failure stiffness, the corresponding Ogden parameters of liver parenchyma identified previously were maintained constant. Typically, curve fitting of the post-failure

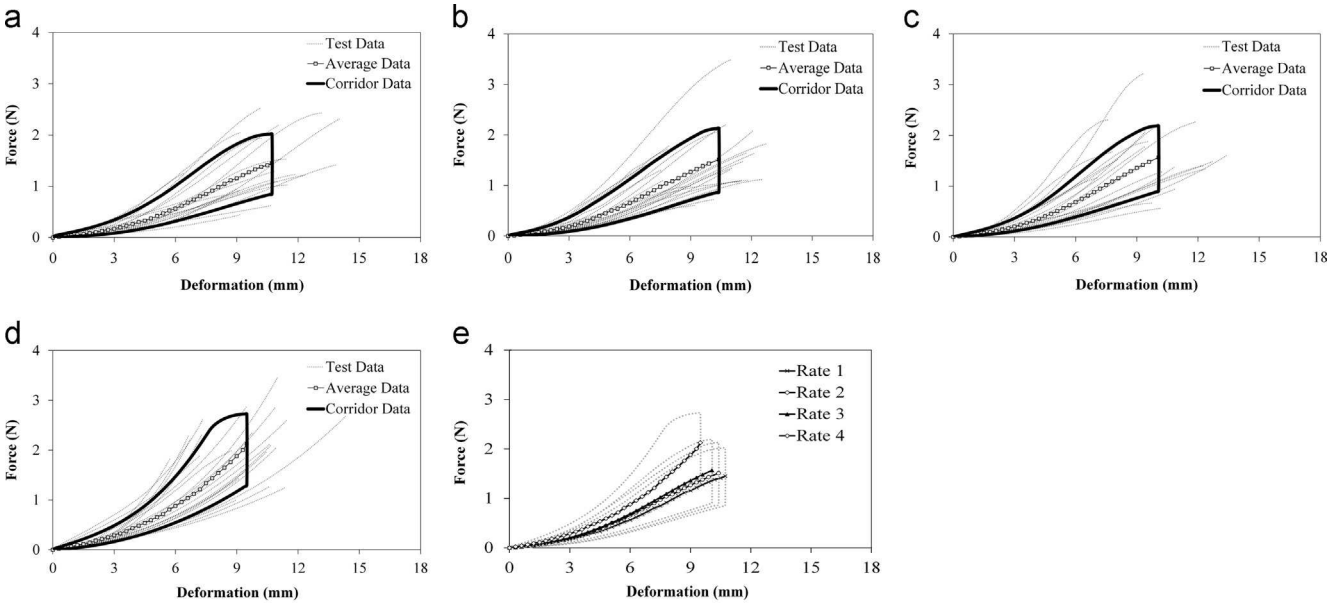

Fig. 4 – Force–deformation curves. Characteristic averages and variation corridors at four loading rates (a) 0.01 s^{-1} (b) 0.1 s^{-1} (c) 1 s^{-1} (d) 10 s^{-1} and (e) all rates (data from current study and Lu et al. 2013 study).

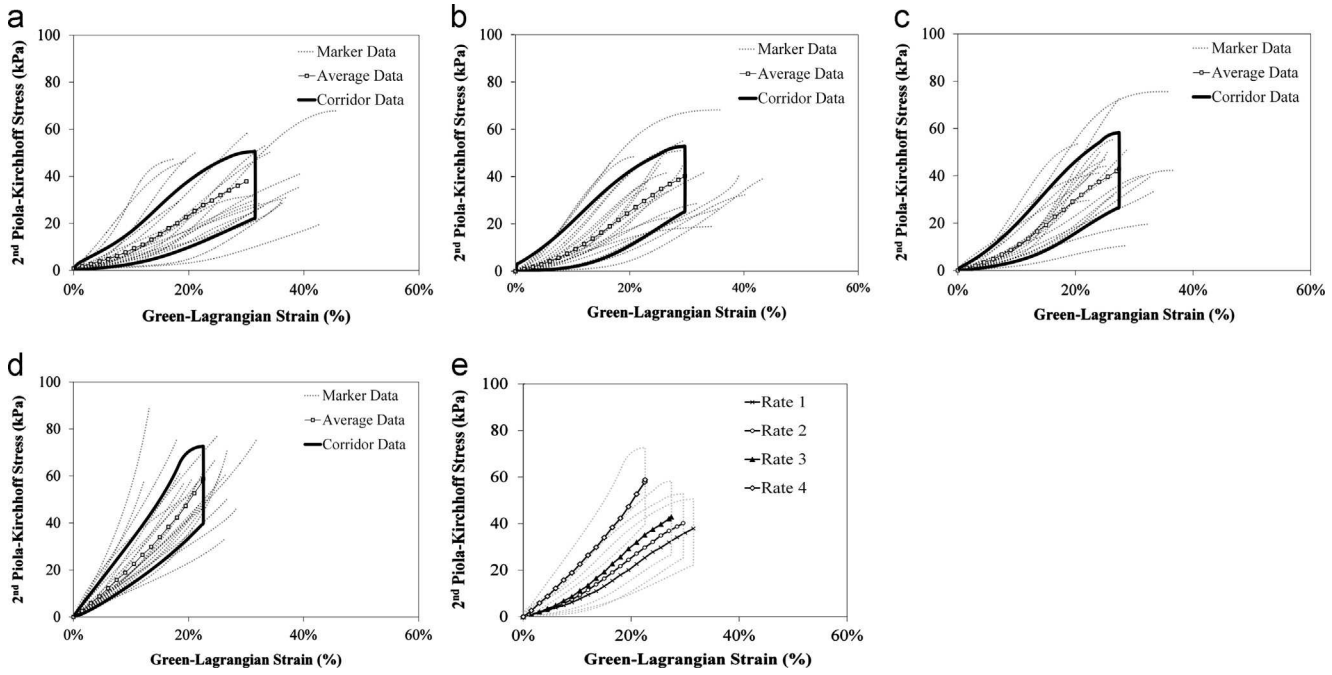

Fig. 5 – Stress–strain curves from the marker model. Characteristic averages and variation corridors at four loading rates (a) 0.01 s^{-1} (b) 0.1 s^{-1} (c) 1 s^{-1} (d) 10 s^{-1} and (e) all rates (data from current study and Lu et al. 2013 study).

Please cite this article as: Untaroiu, C.D., et al., Modeling the biomechanical and injury response of human liver parenchyma under tensile loading. Journal of the Mechanical Behavior of Biomedical Materials (2014), http://dx.doi.org/10.1016/j.jmbbm.2014.07.006

region is challenging using RSM as an objective function, especially after the steep force decline which follows the tear occurrence. Therefore, a "curve mapping" algorithm based on Fréchet distance implemented in LS-Opt was used. In this algorithm the points of one curve were mapped onto the second curve, and the mismatch error, calculated as the area between both curves, is used as an objective function. As in the identification of the parenchyma (bulk) material, the optimization was stopped after six iterations.

3. Results

A total of 34 tensile tests were conducted on parenchyma specimens from two fresh human livers at four different loading rates (0.01 s^{-1}, 0.1 s^{-1}, 1 s^{-1}, and 10 s^{-1}). The average force–deformation curves, average strain–stress curves, and the corresponding variation corridors at each strain rate were quantified. The data in the current study were then combined with the data obtained from three fresh human livers reported in a previous study (Lu et al., 2013) (Figs. 4 and 5).

As in our previous studies (Lu et al., 2013; Untaroiu and Lu, 2013), a typical non-linear behavior was observed in the response of the liver parenchyma (Fig.4). The force–deflection response normally had a toe region followed by an almost linear region. While the pre-failure region usually showed a slight concavity at lower rates, this characteristic was not usually observed in specimens tested at higher rates where the failure occurred mostly within the quasi-linear region.

The values of Ogden material parameters corresponding to each specimen, identified by FE simulation-based optimization, were reported in Table 2. The 2nd PK stress vs. GL strain curves calculated using Ogden material parameters were combined with the previous data obtained from three fresh human livers (Lu et al., 2013) to determine the average strain–stress curves and their variation corridors at each strain rate for the specimen-specific FE models (Fig. 6). The average curves calculated from the marker model and the specimen-specific FE model were further compared with tensile testing data from bovine liver parenchyma (Fig. 6) (Lu et al., 2014). The average Ogden material parameters for each loading rate (Table 2) were identified using the average curves from the specimen-specific FE model data (Fig. 6). The corresponding SD of the model parameters for each loading rate (Table 2) were also determined.

A two-way ANOVA with Tukey–Kramer multiple comparison tests ($\alpha=0.05$) showed that for both the specimen-specific and marker data the means of failure strain and failure stress were significantly different between strain rates ($p<0.05$), and were not significantly different between donors ($p>0.05$) (Table 4). No interaction effects were observed between strain rates and donors ($p>0.05$) (Table 4).

The average values of failure strain and stress were compared (Fig. 7) with corresponding marker data from tensile tests on human liver parenchyma ("human data") (Kemper et al., 2010) and bovine liver parenchyma ("bovine data") (Lu et al., 2014). With an increase in strain rate, all these data demonstrate a decreasing trend in the failure strain (Fig. 7(a)) and an increasing trend in the failure stress (Fig. 7(b)). Two-sample Mann–Whitney tests (Table 3) were performed to compare two data sets at the same rate to

Table 2 – Ogden material parameters obtained using specimen-specific models.

Rate 1	α_1	μ_1	μ	Rate 2	α_1	μ_1	μ	Rate 3	α_1	μ_1	μ	Rate 4	α_1	μ_1	μ
L1-01_4	6.36	5.63	17.91	L2-01_4	9.30	5.31	24.70	L3-01_4	3.38	11.13	18.82	L4-01_4	3.24	12.07	19.53
L1-02_4	3.32	9.26	15.37	L2-02_4	7.01	7.25	25.41	L3-02_4	5.03	11.79	29.66	L4-02_4	3.80	10.34	19.66
L1-03_4	8.00	3.50	14.00	L2-03_4	10.09	4.17	21.05	L3-03_4	2.28.	10.21	11.64	L4-03_4	3.11	12.86	20.01
L1-04_5	5.00	9.80	24.49	L2-04_4	8.23	5.40	22.22	L3-04_4	4.92	13.06	32.11	L4-04_4	3.24	12.78	20.70
L1-05_5	7.62	6.17	23.51	L2-05_4	4.32	13.10	28.32	L3-05_4	2.72	12.29	16.70	L4-05_4	3.13	12.82	20.04
L1-06_5	5.49	14.00	41.19	L2-06_5	7.29	16.73	60.96	L3-06_5	6.19	9.68	29.97	L4-06_5	2.92	19.47	28.38
L1-07_5	5.00	10.95	27.37	L2-07_5	11.14	2.08	11.59	L3-07_5	3.34	14.17	23.69	L4-07_5	2.09	18.92	19.75
				L2-08_5	5.33	8.30	22.10	L3-08_5	8.09	8.65	34.97	L4-08_5	1.75	21.37	18.69
				L2-09_5	12.88	2.93	18.87	L3-09_5	8.66	5.55	24.05	L4-09_5	1.73	19.40	16.83
Mean[a]	8.3	5.84	25.83	Mean[a]	9.06	6.31	30.45	Mean[a]	10.57	5.24	29.69	Mean[a]	11.9	4.7	29.78
SD[a]	0.1	0.00057	9.34	SD[a]	0.085	0.0015	15.99	SD[a]	0.098	0.0025	17.32	SD[a]	0.1	0.0004	13.34

Note: Units: μ_1 (kPa) and (kPa).
[a] The mean and SD data was determined based on data reported in this study and from Lu et al. (2013).

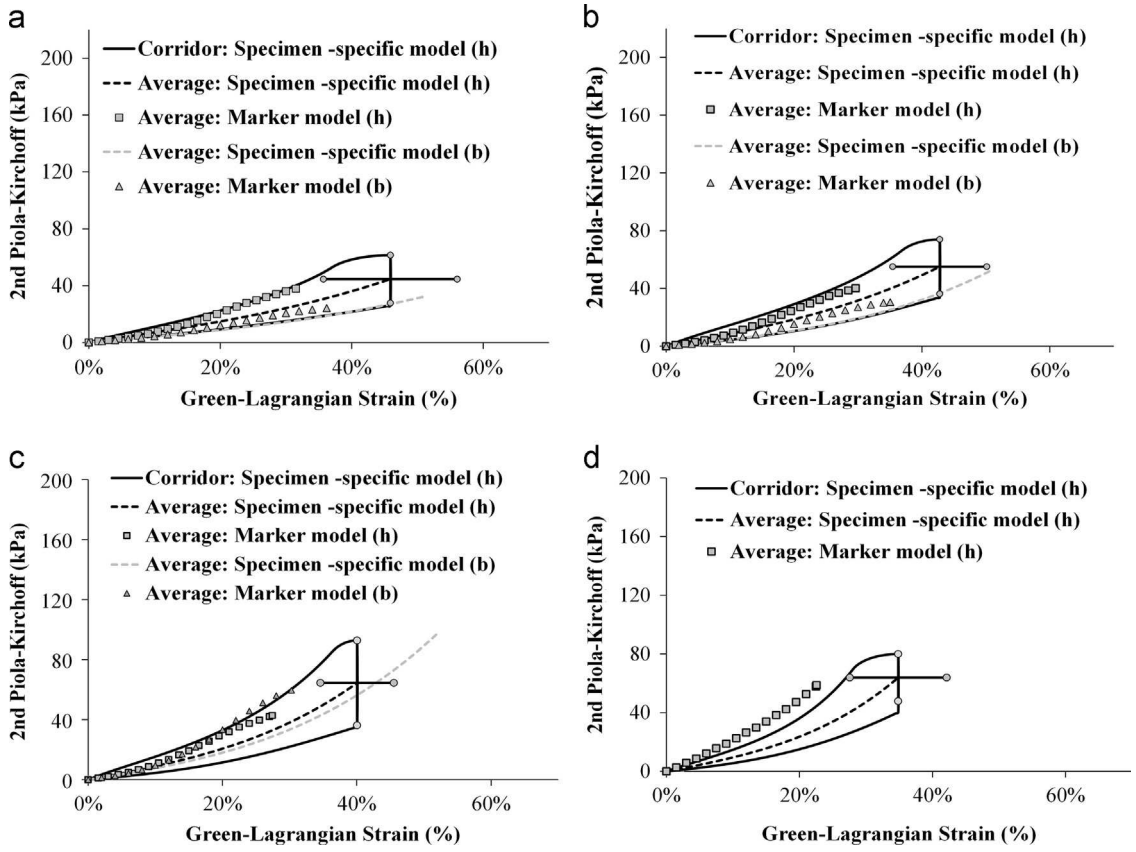

Fig. 6 – Stress–strain curves using the specimen-specific FE model and the marker model from human (h) and bovine (b) specimens (Lu et al. 2014). Characteristic averages and variation corridors at four loading rates (a) 0.01 s^{-1} (b) 0.1 s^{-1} (c) 1 s^{-1} and (d) 10 s^{-1} (data from current study and Lu et al. 2013).

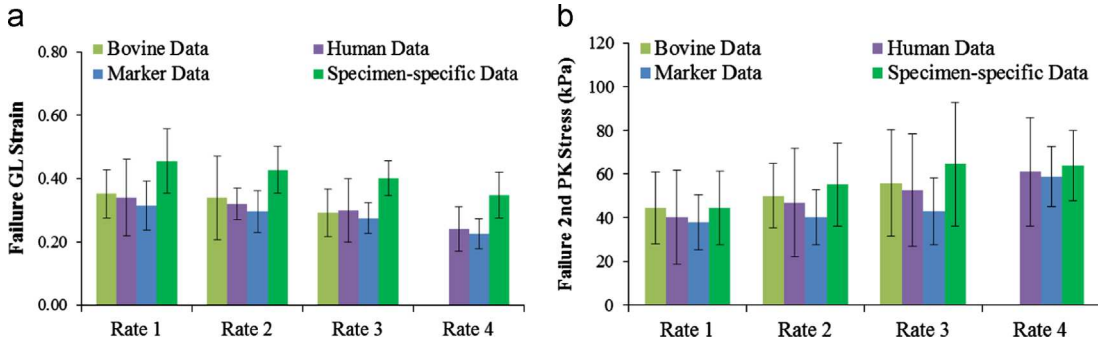

Fig. 7 – Comparison of (a) Green–Lagrangian (GL) failure strain (b) 2nd Piola-Kirchhoff (PK) failure stress: Marker Data vs. Specimen-specific Data vs. Bovine Data (Lu et al. 2014) vs. Human Data (Kemper et al. 2010).

Table 3 – Statistical comparisons between data sets.

Failure strain/failure stress	Rate 1	Rate 2	Rate 3	Rate 4
Specimen-specific vs. marker	**<0.01**/0.12	**<0.01**/**0.1**	**<0.01**/**<0.01**	**<0.01**/0.22
Specimen-specific vs. bovine[a]	**<0.01**/0.91	**0.04**/0.43	**<0.01**/0.22	–
marker vs. bovine[a]	0.19/0.26	0.33/0.06	0.72/0.15	–
marker vs. human[b]	0.55/0.61	0.31/0.31	0.24/0.61	0.42/0.79

Bold: p-value <0.05 indicates significantly different.
[a] Bovine data (Lu et al., 2014) is available only at Rate 1, 2, and 3.
[b] human data (Kemper et al. 2010).

Please cite this article as: Untaroiu, C.D., et al., Modeling the biomechanical and injury response of human liver parenchyma under tensile loading. Journal of the Mechanical Behavior of Biomedical Materials (2014), http://dx.doi.org/10.1016/j.jmbbm.2014.07.006

Table 4 – Two-way ANOVA for testing the effects of strain rates and donors on the mean of the failure strain and failure stress. Bold: p-value <0.05.

Specimen specific model		
Failure strain	p-value	Comparisons ($p<0.05$)
Strain rate	**<0.01**	Rate 1 > Rate 3,4
Donor	0.52	
Rate and donor interaction	0.76	
Failure stress	p-value	Comparisons ($p<0.05$)
Strain rate	**<0.01**	Rate 1,2,3 < Rate 4, Rate 1 < Rate 3
Donor	0.80	
Rate and donor interaction	0.20	
Marker model		
Failure strain	p-value	Comparisons ($p<0.05$)
Strain rate	**<0.01**	Rate 1,2,3 > Rate 4
Donor	0.44	
Rate and donor interaction	0.51	
Failure stress	p-value	Comparisons ($p<0.05$)
Strain rate	**<0.01**	Rate 1,2,3 < Rate4
Donor	0.79	
Rate and donor interaction	0.20	

investigate the possible differences between the models (e.g. marker data vs. specimen-specific data or human data vs. bovine data). No significant differences were found between the marker data in the current study and other marker human data (Kemper et al., 2010) or between the marker human data and the marker bovine data (Lu et al., 2014) for corresponding rate and stress/strain combinations ($p>0.05$). However, significant differences of failure stress and strain were observed between the specimen-specific FE data and the marker data, and the specimen-specific FE data and the marker bovine data ($p<0.05$) (Table 3).

The stress–strain curves predicted by the cube model using the LS-Dyna parenchyma material model at each of the four strain rates used in testing (0.01 s^{-1}, 0.1 s^{-1}, 1 s^{-1}, 10 s^{-1}) showed a good match with the average stress–strain curves of the specimen-specific FE model (Fig. 8). In addition, the stress–strain curves simulated at other different strain rates (0.05 s^{-1}, 0.5 s^{-1}, 5 s^{-1}) showed a similar shape and an increased stiffness with an increase in strain rate. A sensitivity study with respect to the bulk modulus performed using values ranging from 10 MPa to 1000 MPa showed small variation of the tensile force (under 1%) Therefore, a bulk modulus of 320 MPa was used in the simulations of specimen-specific models with CZM.

A reasonable match to the test data was shown by the parenchyma models with CZM added at the tear location (Fig. 9). The pre-failure region optimized previously was not affected by adding the CZM and it maintained a good fit with the test data. The failure of CZM region generates a drop in the grip forces at almost the same time as the test data. The model force time histories reasonably followed the test data after the tear initiation (Fig. 9). While there are some inherent variations in the identified values of maximum traction (σ_{max}) and failure separation (λ_{fail}) (Table 5), some similarities are observed in the normalized traction–separation curves (Fig. 10).

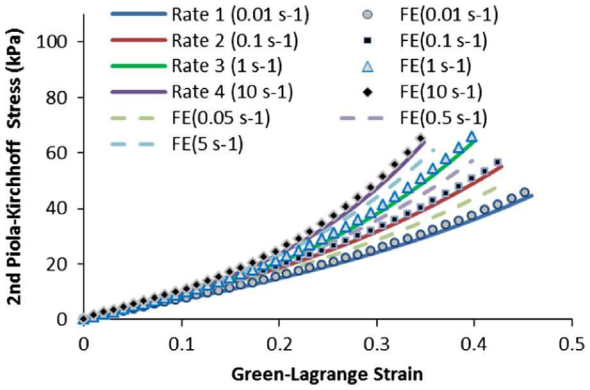

Fig. 8 – Comparison between the stress–strain test data and one element FE predictions.

4. Discussion

The rapid advancement in both computation power and nonlinear FE software has allowed for the possibility to develop accurate human computational models that may avoid the difficulties and cost of Post Mortem Human Surrogate (PMHS) tests used in various biomechanical studies. Recently, several human FE models were developed to better understand the response and injury mechanisms of the human abdomen under impact loading corresponding to automotive accidents (Vavalle et al., 2013; Roth et al., 2013) or ballistic impacts (Shao et al., 2013). In these models, accurate geometries of the human abdomen were reconstructed from human medical images, but the complex material properties of the liver and other solid abdominal organs were usually assigned simplified material models (e.g. elastic model used in Roth et al., 2013) without strain-rate dependency due to a lack of accurate human material property data in literature. It is well known that loading velocity significantly affects overall

Please cite this article as: Untaroiu, C.D., et al., Modeling the biomechanical and injury response of human liver parenchyma under tensile loading. Journal of the Mechanical Behavior of Biomedical Materials (2014), http://dx.doi.org/10.1016/j.jmbbm.2014.07.006

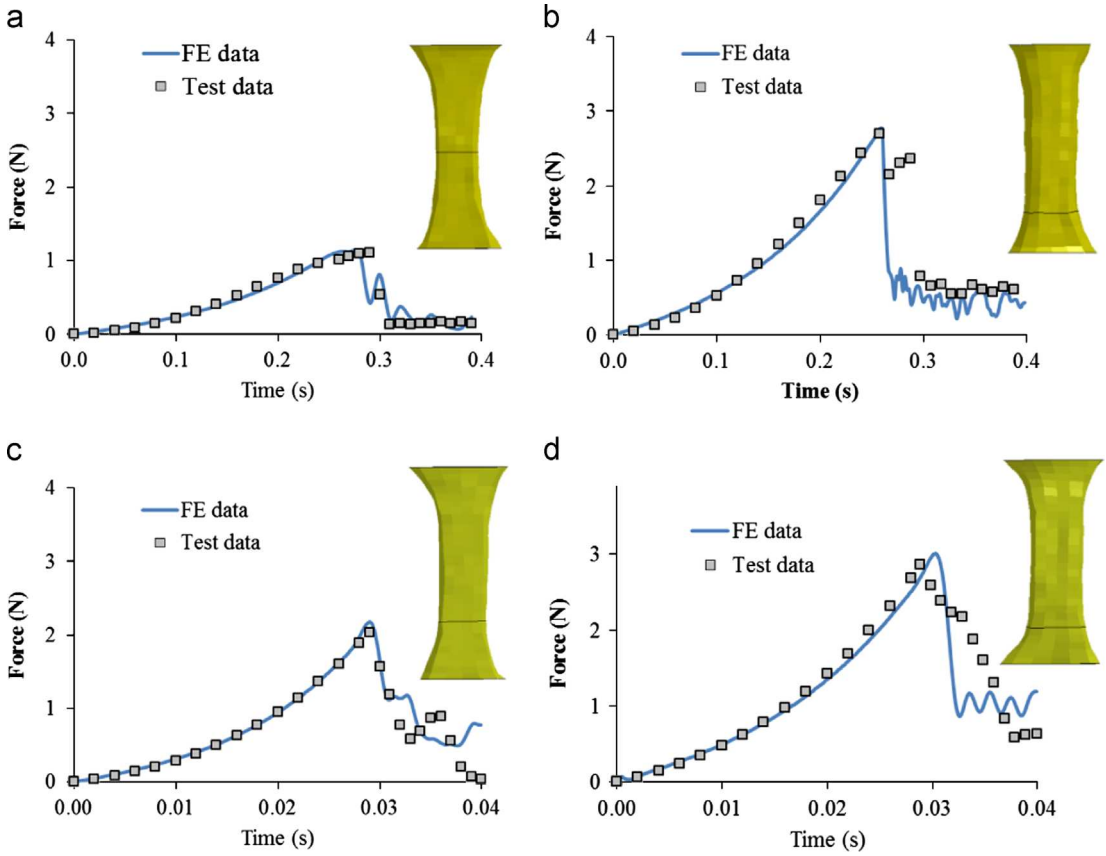

Fig. 9 – Comparison between the test data and the FE data: specimen model with CZM: Representative specimens (a) L3-01_4 (b) L3-02_4 (c) L4-01_4 and (d) L4-02_4.

Table 5 – CZM material parameters.

Specimen units	δ_n^c (mm)	λ_1 (mm)	λ_2 (mm)	λ_{fail} (mm)	σ_{max} (kPa)
L3-01_4	3.87	0.27	0.87	1.85	50.4
L3-02_4	0.42	0.24	0.73	1.58	80.0
L4-01_4	0.17	0.14	0.44	1.14	103.9
L4-02_4	3.53	0.17	0.37	1.53	62.4

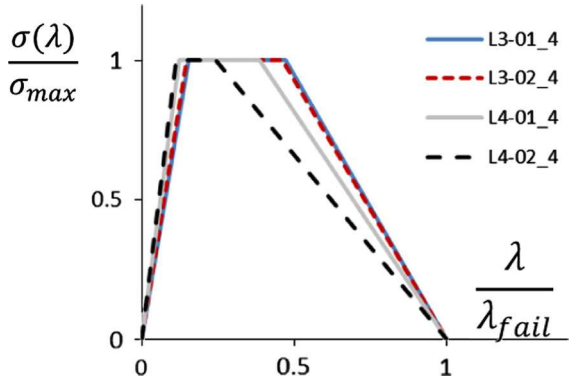

Fig. 10 – The identified traction–separation laws.

human FE model response and injury predictions. Consequently, there is a need for better characterization of human soft tissues especially at higher loading rates. Therefore, the objective of this paper was to investigate the tensile material and failure properties of human liver over a large range of loading rates (0.01–10 s^{-1}). Similar test data reported previously (Lu et al., 2013) was combined with the current data set to yield the average curves and variation corridors from a total of 86 human parenchyma tests.

Typical mechanical characteristics of soft tissues are observed in the structural and material properties of liver parenchyma. Both the force–deformation and the stress–strain relationships exhibit non-linear behavior as well as a dependence on strain rate. As in previous studies (Untaroiu and Lu, 2013; Lu et al., 2013), the average stress–strain curves obtained using the marker model were found to be qualitatively stiffer than the corresponding stress–strain curves obtained by specimen-specific FE models. In addition, significantly larger failure strain and stress were observed in the specimen-specific FE models compared to the marker model. Since both models assume a homogenous and isotropic tissue and use the same grip force time history, it is more likely that the

Please cite this article as: Untaroiu, C.D., et al., Modeling the biomechanical and injury response of human liver parenchyma under tensile loading. Journal of the Mechanical Behavior of Biomedical Materials (2014), http://dx.doi.org/10.1016/j.jmbbm.2014.07.006

differences are due to the modeling approaches used. In the marker model, the strain is calculated based on the marker displacement assuming a uniform strain field between the paint markers. However, geometric irregularities, possible tissue inhomogeneity and the gravity may add some inaccuracies to the calculated strain–stress responses. For example, a non-uniform strain field was recorded using digital image correlation (DIC) technique even on the central portion of liver coupons tested under uniaxial tension (Gao and Desai, 2010). In addition, a non-uniform strain field was also observed in the homogenous and isotropic coupon models during tensile FE simulations caused mostly by the geometric irregularities and boundary conditions. This finding was also reported in previous studies (Untaroiu, 2013; Medina-Cetina and Rechenmacher, 2010; Zhao et al., 2008). On the other hand, the specimen-specific model considers the entire geometry of the specimen and the Ogden parameters, which define the model stress–strain relationship, are changed iteratively until the grip force–time history (global response) fits the corresponding experimental force data. The possible inhomogeneity of the specimen and neglecting of the preload (i.e. initial stress/strain) caused by gravity and compression by the grips may influence the accuracy of the specimen-specific model as well. Although an approach to take into account this preloading in the specimen-specific FE model should be investigated in the future, it should be noted that FE simulations with a human model are typically performed without pre-loading of internal organs. Therefore, the material properties provided in this study could be used in this type of simulation set-up. In many studies, material inhomogeneity in human hard tissues (e.g. bone) is typically considered in the numerical models by various relationships with apparent tissue density, mineral density, or porosity (Rudy et al., 2011). However, to the authors' knowledge, similar studies for human soft tissues are lacking in the literature. Therefore, future studies may further investigate inhomogeneity in soft tissue and implement it in numerical models.

CZM has been used extensively to predict failure in different materials, but its use in predicting failures in soft materials is limited (Bhattacharjee et al., 2013). In this study, the CZM approach was used to simulate the failure (tear) propagation path through the liver parenchyma during failure tests. Overall, the model with optimized CZM parameters matched well with the time history of the grip force after the failure occurred. Although this work was a pilot study, simulation of additional tests with various types of CZM separation-laws and other modeling approaches, such as the extended FE method (XFEM) (Pannachet et al., 2009; Menk, SPA. (2010)), are planned to be performed in the future.

This study has some limitations. The liver is perfused with blood under physiological conditions which may add some dilatation that is not present in the liver specimens tested in this study. A previous study reported (Kerdok et al., 2006) that un-perfused livers have a higher stiffness than perfused livers. However, no data exist for dynamic in vivo loading, especially in respect to failure. Therefore, the effects of perfusion on dynamic material properties of liver should be addressed in future studies.

In the current work, as in previous studies that used CZM to model failure (Bhattacharjee et al., 2013), the path of the tear was assumed to be known. Therefore, the CZM elements were developed perpendicular to the direction of loading at tear location. However, for a liver model included in a full human body model, the tear location and propagation is not known *a priori*. Therefore, CZM elements should be developed in the whole liver FE model between all liver parenchyma elements. Based on our knowledge, an automatic methodology for the generation of these CZM elements is lacking in current software packages, and therefore should be developed in the future. In addition, due to the lack of data, the CZM parameters and their ranges were chosen in an ad hoc manner in the optimization. This approach was found to be reasonable for uni-axial tensile tests; however, more work is needed to generalize the CZM approach for the simulation of complex loading. For example, additional testing that focuses on the detection and recording of the tearing process should be performed under various loading conditions (tension, shear, and compression). While the CZM has been used to model crack propagation(injury) under shear and tensile loading, the overlapping zone modeling (OZM) was recently proposed for modeling crack propagation (injury) generated by compression and shear loading (Carpinteri et al., 2012). In a close analogy with CZM, the localized compressive behavior is modeled using a compressive stress vs. interpenetration law. To identify the law parameters corresponding to liver parenchyma, additional compression testing focused on injury detection should be performed.

During an automobile crash, the abdomen could be subjected to combined loading (e.g. tension, compression and shear) due to the contact with the belt system and vehicle interior parts. This loading is transferred to abdominal organs and may result in a complex stress distribution within the liver. The results of dynamic compression tests on perfused whole human livers using a large flat loading surface attached to a drop tower were previously reported (Sparks et al., 2007). The experimental injury outcome included injuries caused by both tensile and compressive loading such as capsule/parenchyma lacerations and intra-parenchymal damage, respectively. These experimentally induced liver injuries were consistent with those documented in the Crash Injury Research and Engineering Network (CIREN) database (Sparks et al., 2007). In the current study, both identified material and failure models are based only on data recorded in tensile tests. Therefore, in future, the proposed material model of liver parenchyma (MAT 181) should be improved by adding the compressive stress–strain curves for various strain rates obtained from literature (Kemper et al., 2013) or from new test data.

5. Conclusions

A strain rate dependent material model and a failure model for human liver parenchyma were proposed in this study. The data from 32 new uniaxial tensile tests performed at four different loading rates on fresh specimens of human liver parenchyma were combined with previously published data to calculate the statistical distributions of model parameters (averages and SD). In addition, the values of failure stress and strain based on marker and specimen-specific FE models

Please cite this article as: Untaroiu, C.D., et al., Modeling the biomechanical and injury response of human liver parenchyma under tensile loading. Journal of the Mechanical Behavior of Biomedical Materials (2014), http://dx.doi.org/10.1016/j.jmbbm.2014.07.006

were identified for each test, as well as their statistical comparisons. Overall, the failure stress increased with increased loading rate, while the failure strain decreased with increased loading rate. The cohesive zone modeling (CZM) approach, used to model tearing process, showed promising results in terms of modeling the post-failure force time history response at higher loading rates. All mechanical and failure data reported in this study could be easily implemented in human liver models to help identify the mechanisms of liver injuries during vehicle collisions, and possibly aid in the development of advanced protective systems (Adam and Untaroiu, 2011; Untaroiu and Adam, 2013).

REFERENCES

Adam, T., Untaroiu, C.D., 2011. Identification of occupant posture using a bayesian classification methodology to reduce the risk of injury in a collision. Transport. Res. Part C: Emer. Tech. 19, 1078–1094.

Ahmed, I, Beckingham, I., 2007. Liver trauma. Trauma 9, 171–180.

Behr, M., Arnoux, J.B., Serre, T., et al., 2003. A human model for road safety: from geometrical acquisition to model validation with Radioss. Comput. Methods Biomech. Biomed. Eng. 6, 263–273.

Benzeggagh, M.L., Kenane, M., 1996. Measurement of mixed-mode delamination fracture toughness of unidirectional glass/epoxy composites with mixed-mode bending apparatus. Comp. Sci. Technol. 56, 439–449.

Bhattacharjee, T., Barlingay, M., Tasneem, H., et al., 2013. Cohesive zone modeling of mode I tearing in thin soft materials. J. Mech. Behav. Biomed. Mater. 28, 37–46.

Brunon, A., Bruyere-Garnier, K., Coret, M., 2010. Mechanical characterization of liver capsule through uniaxial quasi-static tensile tests until failure. J. Biomech. 43, 2221–2227.

Camacho, G.T., Ortiz, M., 1996. Computational modeling of impact damage in brittle materials. Int. J. Solids Struct. 33, 2899–2938.

Carpinteri, A., Gong, B.M., Corrado, M., 2012. Hardening cohesive/overlapping zone model for metallic materials: the size-scale independent constitutive law. Eng. Fract. Mech. 82, 29–45.

Chui, C., Kobayashi, E., Chen, X., et al., 2007. Transversely isotropic properties of porcine liver tissue: experiments and constitutive modeling. Med. Biol. Eng. Comput. 45, 99–106.

Cox, B.N., Gao, H.J., Gross, D., et al., 2005. Modern topics and challenges in dynamic fracture. J. Mech. Phys. Solids 53, 565–596.

Gao, Z., Desai, J.P., 2010. Estimating zero-strain states of very soft tissue under gravity loading using digital image correlation. Med. Image Anal. 14, 126–137.

Gao, Z., Lister, K., Desai, J.P., 2010. Constitutive modeling of liver tissue: experiment and theory. Ann. Biomed. Eng. 38, 505–516.

Guinea, G.V., Planas, J., Elices, M., 1994. A general bilinear fit for the softening curve of concrete. Mater. Struct. 27, 99–105.

Hallquist, J.O., 2006. In: LS-DYNA Theory Manual, LSTC.

Harbrecht, B.G., Peitzman, A.B., Rivera, L., et al., 2001. Contribution of age and gender to outcome of blunt splenic injury in adults: multicenter study of the eastern association for the surgery of trauma. J. Trauma 51, 887–895.

Hollenstein, M., Nava, A., Valtorta, D., et al., 2006. Mechanical characterization of the liver capsule and parenchyma. In: Harders, M., Székely, G. (Eds.), Biomedical Simulation. Springer, Berlin Heidelberg, pp. 150–158.

Howes, M.K., Gregory, T.S., Hardy, W.N., et al., 2012. Kinematics of the thoraco–abdominal contents under various loading scenarios. Stapp Car Crash J. 56, 1–48.

Hu, J., Klinich, K.D., Miller, C.S., et al., 2009. Quantifying dynamic mechanical properties of human placenta tissue using optimization techniques with specimen-specific finite-element models. J. Biomech. 42, 2528–2534.

Hu, J., Klinich, K.D., Miller, C.S., et al., 2011. A stochastic visco-hyperelastic model of human placenta tissue for finite element crash simulations. Ann. Biomed. Eng. 39, 1074–1083.

Jin, W., Deng, L., Lv, H., et al., 2013. Mechanisms of blunt liver trauma patterns: an analysis of 53 cases. Exp. Ther. Med. 5, 395–398.

Kanninen, M.F., Popelar, C.H., 1985. Advanced Fracture Mechanics. Oxford University Press, New York.

Kemper, A.R., Santago, A.C., Stitzel, J.D., et al., 2010. Biomechanical response of human liver in tensile loading. Ann. Adv. Automot. Med. 54, 15–26.

Kemper, A.R., Santago, A.C., Stitzel, J.D., et al., 2013. Effect of strain rate on the material properties of human liver parenchyma in unconfined compression. J. Biomech. Eng. 135, 104503–104508.

Kerdok, A.E., Ottensmeyer, M.P., Howe, R.D., 2006. Effects of perfusion on the viscoelastic characteristics of liver. J. Biomech. 39, 2221–2231.

Kolling, S., Bois, P.A.D., Benson, D.J., et al., 2007. A tabulated formulation of hyperelasticity with rate effects and damage. Comput. Mech. 40, 885–899.

Lu, Y-C, Untaroiu, C.D., 2013. Effect of storage methods on indentation-based material properties of abdominal organs due to tissue storage methods. J. Eng. Med., Proc IMechE-Part H 227, 293–301.

Lu, Y.C., Kemper, A.R., Gayzik, S., et al., 2013. Statistical modeling of human liver incorporating the variations in shape, size, and material properties. Stapp Car Crash J. 57, 285–311.

Lu, Y.C., Kemper, A.R., Untaroiu, C.D., 2014. Effect of storage on tensile material properties of bovine liver. J. Mech. Behav. Biomed. Mater. 29, 339–349.

Medina-Cetina, Z., Rechenmacher, A., 2010. Influence of boundary conditions, specimen geometry and material heterogeneity on model calibration from triaxial tests. Int. J. Numer. Anal. Methods Geomech. 34, 627–643.

Menk, A., S.P.A., Bordas, 2010. Numerically determined enrichment functions for the extended finite element method and applications to bi-material anisotropic fracture and polycrystals. Int. J. Numer. Methods Eng. 83, 805–828.

Nahum, A.M., Melvin, J.W., 2002. In: Accidental Injury: Biomechanics And Prevention. Springer.

Ortiz, M., Pandolfi, A., 1999. Finite-deformation irreversible cohesive elements for three-dimensional crack-propagation analysis. Int. J. Numer. Methods Eng. 44, 1267–1282.

Pannachet, T, Sluys, L.J., Askes, H., 2009. Error estimation and adaptivity for discontinuous failure. Int. J. Numer. Methods Eng. 78, 528–563.

Park, K., Paulino, G.H., 2013. Cohesive zone models: a critical review of traction–separation relationships across fracture surfaces. Appl. Mech. Rev. 64, 060802.

Rainsberger, R., 2006. TrueGrid User's Manual.

Roth, S., Torres, F., Feuerstein, P., et al., 2013. Anthropometric dependence of the response of a Thorax FE model under high speed loading: validation and real world accident replication. Comput. Methods Progr. Biomed. 110, 160–170.

Rudy, D.J., Deuerling, J.M., Orias, A.A.E., et al., 2011. Anatomic variation in the elastic inhomogeneity and anisotropy of human femoral cortical bone tissue is consistent across multiple donors. J. Biomech. 44, 1817–1820.

Santago, A.C., Kemper, A.R., McNally, C, et al., 2009a. Freezing affects the mechanical properties of bovine liver. Biomed. Sci. Instrum. 45, 24–29.

Santago, A.C., Kemper, A.R., McNally, C., et al., 2009b. The effect of temperature on the mechanical properties of bovine liver. Biomed. Sci. Instrum. 45, 376–381.

Please cite this article as: Untaroiu, C.D., et al., Modeling the biomechanical and injury response of human liver parenchyma under tensile loading. Journal of the Mechanical Behavior of Biomedical Materials (2014), http://dx.doi.org/10.1016/j.jmbbm.2014.07.006

Shao, Y., Zou, D.H., Li, Z.D., et al., 2013. Blunt liver injury with intact ribs under impacts on the abdomen: a biomechanical investigation. Plos One, 8.

Snedeker, J.G., Niederer, P., Schmidlin, F.R., et al., 2005. Strain-rate dependent material properties of the porcine and human kidney capsule. J. Biomech. 38, 1011–1021.

Sparks, JL, JHt, Bolte, Dupaix, RB, et al., 2007. Using pressure to predict liver injury risk from blunt impact. Stapp Car Crash J. 51, 401–432.

Tvergaard, V., 1990. Effect of fiber debonding in a whisker-reinforced metal. Mater. Sci. Eng.-Struct. Mater. Prop Microstruct. Process. 125, 203–213.

Tvergaard, V, Hutchinson, J.W., 1992. The relation between crack-growth resistance and fracture process parameters in elastic plastic solids. J. Mech. Phys. Solids 40, 1377–1397.

Tvergaard, V., Hutchinson, J.W., 1993. The influence of plasticity on mixed-mode interface toughness. J. Mech. Phys. Solids 41, 1119–1135.

Umale, S., Deck, C., Bourdet, N., et al., 2013. Experimental mechanical characterization of abdominal organs: liver, kidney & spleen. J. Mech. Behav. Biomed. Mater. 17, 22–33.

Untaroiu, C.D., 2013. The influence of the specimen shape and loading conditions on the parameter identification of a viscoelastic brain model. Comput. Math Methods Med. 2013, 460413.

Untaroiu, C.D., Adam, T., 2013. Performance-based classification of occupant posture to reduce the risk of injury in a collision. IEEE Trans. Intel. Transport. Sys. 14, 565–573.

Untaroiu, C.D., Lu, Y-C., 2013. Material characterization of liver parenchyma using specimen-specific finite element models. J. Mech. Behav. Biomed. Mater. 26, 11–22.

Vavalle, N.A., Moreno, D.P., Rhyne, A.C., et al., 2013. Lateral Impact Validation of a Geometrically Accurate Full Body Finite Element Model for Blunt Injury Prediction. Ann. Biomed. Eng. 41, 497–512.

Yamada, H., 1970. In: Strength of Biological Materials. Williams and Wilkins, Huntingdon, NY.

Zhao, Y.H., Guo, Y.Z., Wei, Q., et al., 2008. Influence of specimen dimensions on the tensile behavior of ultrafine-grained Cu. Scr. Mater. 59, 627–630.

Please cite this article as: Untaroiu, C.D., et al., Modeling the biomechanical and injury response of human liver parenchyma under tensile loading. Journal of the Mechanical Behavior of Biomedical Materials (2014), http://dx.doi.org/10.1016/j.jmbbm.2014.07.006